THE ANNALS OF "DUNAREA DE JOS" UNIVERSITY OF GALATI
FASCICLE IX. METALLURGY AND MATERIALS SCIENCE
No. 1 - 2026, ISSN 2668-4748; e-ISSN 2668-4756
Article DOI: https://doi.org/10.35219/mms.2026.1.02

FAILURE CASE STUDY SERIES PART ONE: ANALYSIS OF OXYGEN COMPRESSOR SHAFT BREAKAGE

Liviu GURĂU, Carmela GURĂU, Gheorghe GURĂU
Interdisciplinary Research Centre in the Field of Eco-Nano Technology and Advanced Materials CC-ITI, Faculty of Engineering, "Dunarea de Jos" University of Galati, 47 Domneasca Street, 800008 Galati, Romania
e-mail: gheorghe.gurau@ugal.ro

ABSTRACT

This paper presents the results of a failure analysis of an oxygen compressor shaft using seven basic steps. The findings of this work form the basis for corrective and preventive actions to enhance equipment reliability and prevent future recurrence. The paper also offers a simple and direct approach to determine the root cause of structural component failure.

Visual inspection, specimen selection and preservation, high-stress area identification, chemical analysis with comparison to standards, hardness testing, optical microscopy, scanning electron microscopy (SEM), and EDS analysis were performed. A comprehensive metallurgical analysis of the oxygen compressor shaft failure provided substantial insights into the underlying mechanism, indicating shaft misalignment and bending-induced fatigue as the primary causes, with poor steel quality contributing to faster crack initiation and propagation.

KEYWORDS: failure analysis, fatigue, compressor shaft, OM, SEM, EDS

1. Introduction

The compressor crankshaft is a critical rotating component that converts the reciprocating motion of the pistons into rotary motion, enabling the continuous compression of oxygen gas [1]. Typically manufactured from high-strength forged steel, the crankshaft is designed to withstand cyclic stress [2, 3], torsional loads, and high operating pressures under continuous service. Failure of this component can cause significant secondary damage to associated parts such as bearings, connecting rods, and the housing.

Failure occurs when mechanical components lose their designed functionality under various stresses, such as mechanical loads, thermal stresses, corrosion, or combined effects [4, 5]. Primary tools for shaft failure analysis include visual inspection, optical microscopy, scanning electron microscopy (SEM), metallurgical analysis, and mechanical testing [6-8].

Fatigue is a progressive and localized structural damage mechanism [9-11] that occurs when a material is subjected to cyclic or fluctuating stresses, typically at magnitudes significantly below its ultimate tensile strength (UTS) or yield strength [9, 12, 13]. Under repeated loading–unloading cycles, microscopic defects within the material—such as dislocations, inclusions, or surface irregularities—serve as stress concentrators and evolve into fatigue cracks [14-16].

The main objective of this research is to determine the sequence of events, specifically whether the Shaft failure occurred first or if bearing damage initiated the failure, and to identify the root causes and contributing factors [8].

2. Experimental procedure

The chemical composition was determined by spectral testing using Thermo Scientific ARL 3460 Advantage. The ARL 3460 optical emission spectrometer has been specifically configured to address the analytical requirements for a wide range of alloys. It is driven by the OXSAS analytical software, which provides simple one-click routine analysis launch and full traceability. The test was performed in accordance with ASTM E415-21 for the analysis of carbon and low-alloy steels using spark atomic emission spectrometry. The method facilitates the simultaneous determination of 21 alloying and residual elements in carbon and low-alloy steels.

The hardness test was performed using the KB150 R - Digital Rockwell universal hardness testing machine. This machine is designed for automatic hardness testing and operates within a load

THE ANNALS OF "DUNAREA DE JOS" UNIVERSITY OF GALATI
FASCICLE IX. METALLURGY AND MATERIALS SCIENCE
Nº. 1 - 2026, ISSN 2668-4748; e-ISSN 2668-4756
Article DOI: https://doi.org/10.35219/mms.2026.1.02

range from 1 to 2500 (N), and is used for Rockwell, superficial Rockwell, and depth measurements for Vickers and Brinell tests.

Stereomicroscopy plays a crucial role in failure analysis. The Nikon SMZ745 stereoscopic microscope was employed for low-magnification observation of failure surface.

Optical microscopy was performed using the Olympus GX51 metallurgical microscope, widely used in automotive, aerospace, metallurgy, and research laboratories for precise material characterization and failure analysis. The cross-sectional sample was polished up to 1500 emery grade, followed by 1µm velvet cloth polishing, and then etched using a 2% Nital solution to reveal the microstructures.

Scanning electron microscopy (SEM) and energy dispersive X-ray spectroscopy (EDS) were carried out on the cross-sectional fractured surface of the sample using the JEOL IT-300LV Scanning Electron Microscope. To identify and quantify elemental composition of materials at microscopic scales, the Bruker Energy-Dispersive X-ray Spectroscopy (EDS) system integrated into JEOL SEM was employed.

3. Results and discussion

3.1. Visual inspection

The visual inspection was conducted on the failed compressor components to evaluate the condition of the shaft, bearings, and housing sleeve. The objective was to identify signs of damage, wear patterns, and fracture characteristics that could help determine the root cause of failure. Detailed observations were recorded and supported by photographs (Figure 1) to facilitate subsequent analysis.

Fig. 1. *The fracture surface*

The images show a catastrophic shaft fracture near the bearing region. The fracture surface exhibits fatigue leading to catastrophic failure. The bearing shows complete structural failure, with the rolling elements deformed and displaced from their original positions.

The visual inspection indicates that the compressor shaft experienced a catastrophic fatigue fracture near the bearing and coupling region. The bearing adjacent to the fracture shows complete structural failure, with severe deformation and displacement of the bearing elements, implying a loss of internal alignment and a potential seizure.

3.2. Chemical Composition - Spectral Test

The chemical composition (Table 1) indicates a steel grade similar to 42CrMo4 EN10083/3 (2006). Spectro analysis revealed high sulphur, since no calcium was added during processing, the inclusions remain unmodified and elongated, which may act as stress concentrators.

Typical applications of grade 42CrMo4 EN10083/3 (2006) are: compressor and turbine shafts, aircraft landing gear and engine components, crankshafts, connecting rods, transmission shafts, heavy-duty fasteners, and high-stress structural parts. The key features of this steel are: high strength and toughness over a wide temperature range, excellent fatigue and impact resistance, good hardenability with deep case formation, and moderate corrosion resistance.

THE ANNALS OF "DUNAREA DE JOS" UNIVERSITY OF GALATI
FASCICLE IX. METALLURGY AND MATERIALS SCIENCE
No. 1 - 2026, ISSN 2668-4748; e-ISSN 2668-4756
Article DOI: https://doi.org/10.35219/mms.2026.1.02

Table 1. *Shaft chemical composition*

Element	Compressor Shaft	42CrMo4 EN10083/3 2006	Remarks
Carbon (C)	0.415	0.38–0.45	Within range
Silicon (Si)	0.205	≤0.40	Within range
Manganese (Mn)	0.717	0.60–0.90	Within range
Phosphorus (P)	0.0073	≤0.025	Acceptable
Sulfur (S)	0.0256	≤0.035	**High - not favorable**
Nitrogen (N)	0.0081	—	Acceptable
Chromium (Cr)	0.865	0.90 – 1.20	Acceptable
Molybdenum (Mo)	0.181	0.15–0.30	Within range
Nickel (Ni)	0.747	-	Acceptable
Calcium (Ca)	0.0	—	**No Ca –** inclusions unmodified to globular
Aluminum (Al)	0.0012	≤0.05	Within limit
Vanadium (V)	0.0042	≤0.05	Trace
Titanium (Ti)	0.0027	≤0.05	Trace
Coper (Cu)	0.167	≤0.35	**High - not favorable**
Niobium (Nb)	0.0017	—	Trace
Borom (B)	0.00033	≤0.003	Within limit
CEV	0.80	—	

3.3. Hardness test

The test method used for the blade sample pieces was Vickers Hardness (30) in accordance with the ASTM E92 standard. The resulting value was converted to HB (Brinnel) and HRB (Rockwell). The Vickers 30 (HV 30) test is a highly precise method for measuring material hardness under a 300 N load. It is widely used in metallurgical testing, quality control, and failure analysis to assess the durability and wear resistance of components.

The hardness test was performed 10 mm away from the fracture surface to assess the material's baseline mechanical properties and minimize the influence of deformation or thermal effects near the fracture. This ensures the measured hardness reflects the true condition of the shaft material.

The shaft material exhibited a hardness of 257 HV, consistent with typical values for medium-carbon or heat-treated steels used in fatigue-loaded components. This value falls within the typical range of 250–300 HV, suggesting that the material maintained its expected strength and was not significantly softened.

3.4. Stereomicroscopy

The fracture surface indicates fatigue failure under bending stress. The crack initiated at the outer surface and propagated progressively, as evidenced by the concentric beach marks. The presence of a fibrous region signifies the rapid final fracture that occurred when the remaining cross-section could no longer sustain the applied load. The non-radial alignment of the fibrous region relative to the point of initiation further confirms asymmetric bending - rather than symmetric stress - as the dominant loading condition. Overall, the observed features - initiation site, beach marks, and final rupture are fully consistent with a fatigue-induced fracture mechanism under cyclic bending.

THE ANNALS OF "DUNAREA DE JOS" UNIVERSITY OF GALATI
FASCICLE IX. METALLURGY AND MATERIALS SCIENCE
Nº. 1 - 2026, ISSN 2668-4748; e-ISSN 2668-4756
Article DOI: https://doi.org/10.35219/mms.2026.1.02

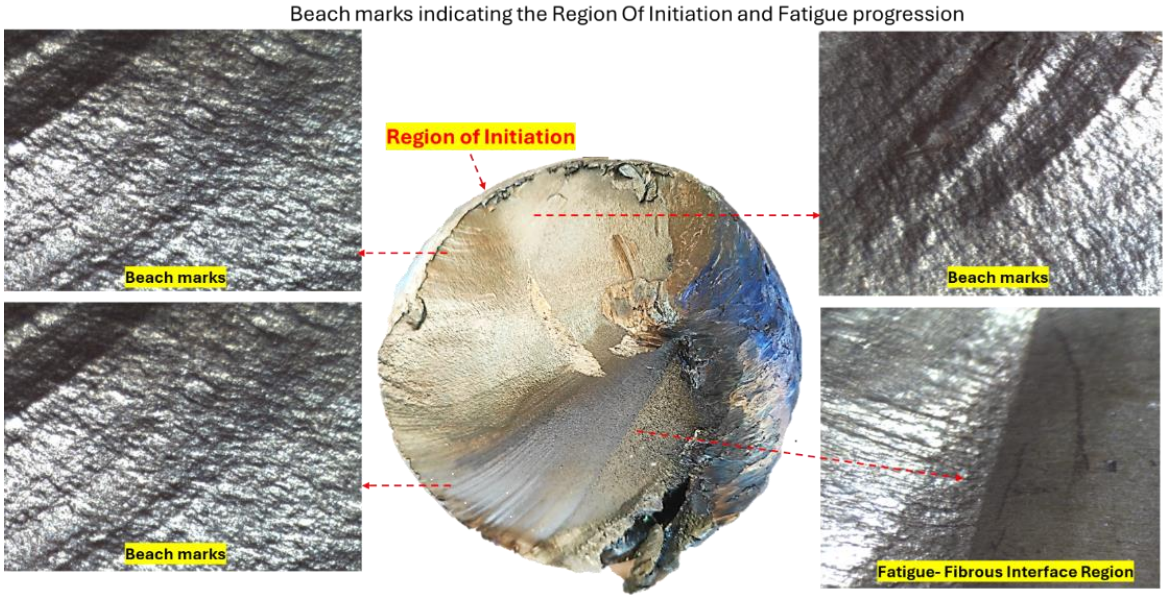

Fig. 2. *Stereomicroscopy images on different zones on failure surface*

3.5. Optical microscopy

The cross-sectional samples (Figure 3) were hot-mounted in phenolic resin. After grinding and polishing, the samples were etched (using 2% nital) and examined for microstructural inferences.

Figure 3b points out a homogenous, fine ferrite-pearlite structure.

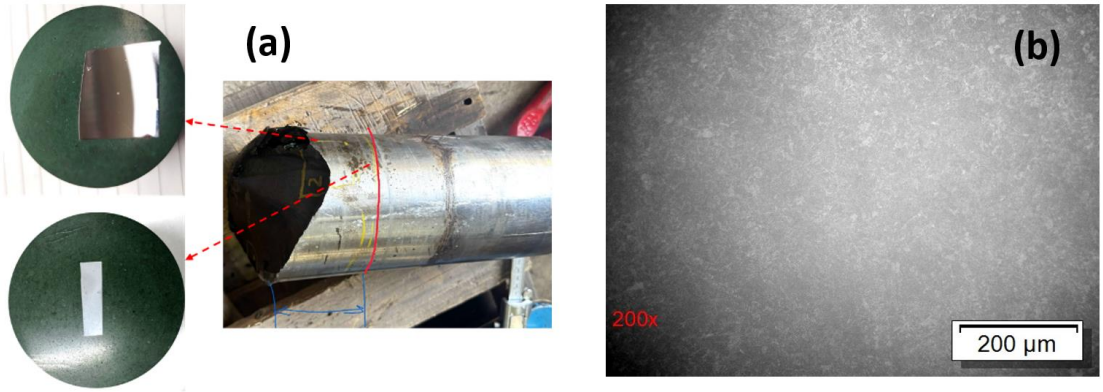

Fig. 3. *Cross-sectional samples (a), ferrite-pearlite structure*

3.6. SEM investigations

SEM was used for fractography analysis to reveal microscopic features such as dimples, cleavage facets, beach marks, and striations that indicated fracture modes and root causes of material failure. Additionally, it was used to detect inclusions, impurities, segregation, porosity, and other processing defects acting as stress concentrators.

EDS was used to measure the weight percentage of all elements present in the defect area. Furthermore, elemental distribution maps clearly visualized element segregation, diffusion, inclusions, and contaminants. Quantitative data reports with precise elemental percentages including spectra, maps, and line profiles were generated.

Ratchet marks were observed that indicate multiple crack planes merging with one another (Figure 4a and b). Moreover, Figure 4c and d show multiple striation indicating progressive fatigue crack growth under cyclic loading.

On further examination, we can observe a coarse exogenous inclusion (0.72 mm) at a depth of 0.80 mm from the surface, located precisely at the region of crack initiation. This inclusion likely acted as a stress concentrator, contributing to the onset of fatigue failure.

THE ANNALS OF "DUNAREA DE JOS" UNIVERSITY OF GALATI
FASCICLE IX. METALLURGY AND MATERIALS SCIENCE
No. 1 - 2026, ISSN 2668-4748; e-ISSN 2668-4756
Article DOI: https://doi.org/10.35219/mms.2026.1.02

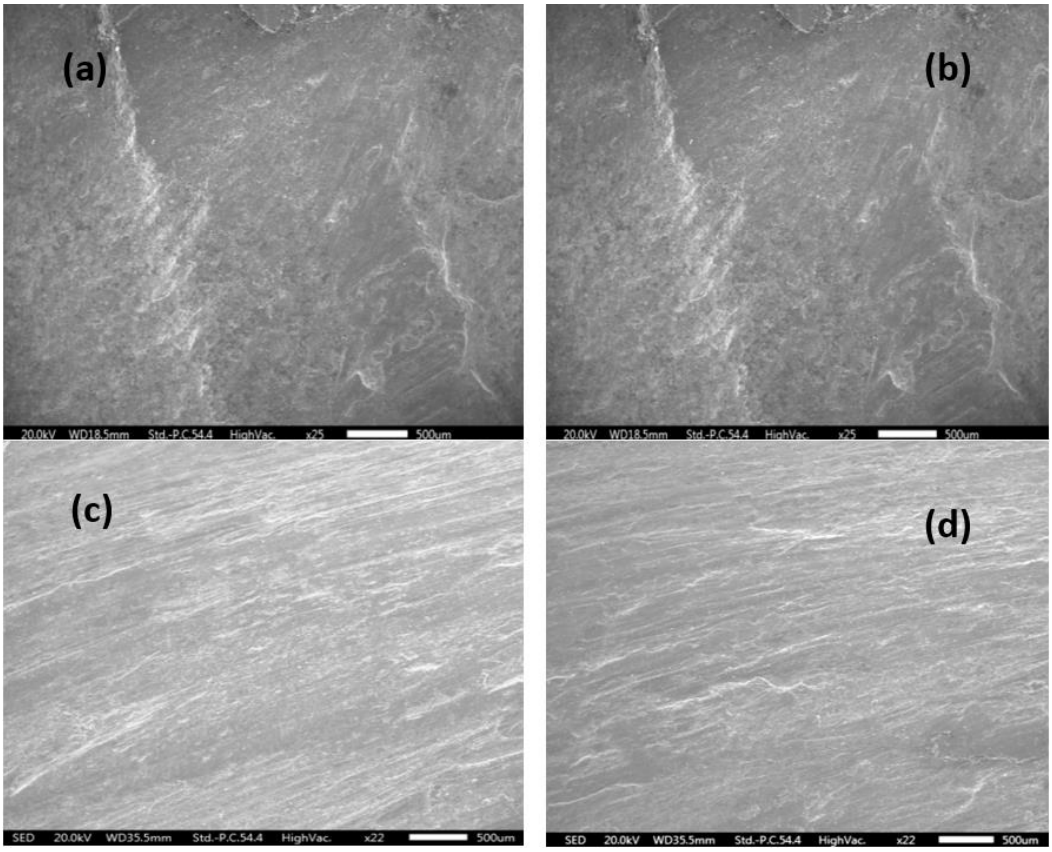

Fig. 4. *SEM micrographs*

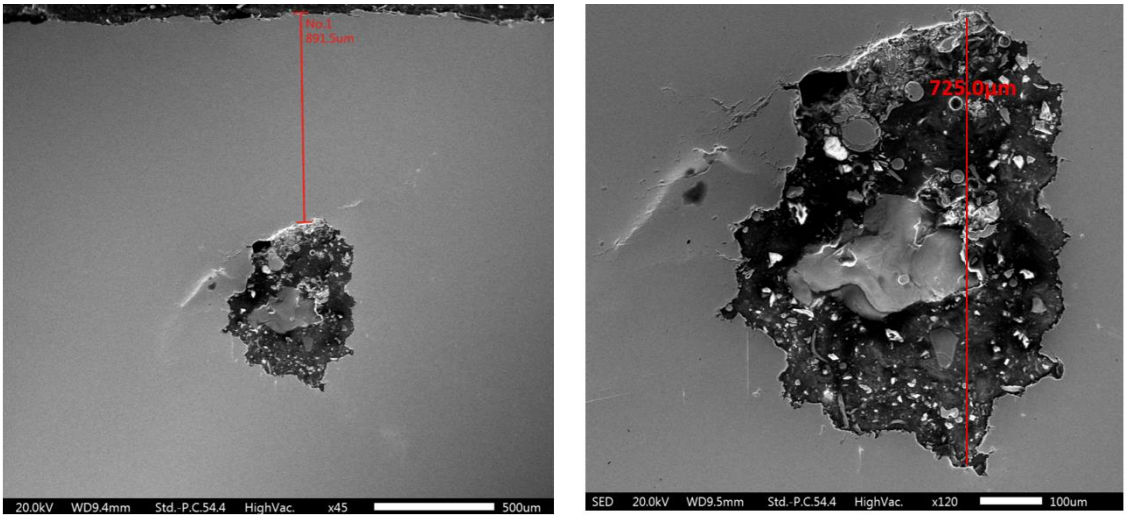

Fig. 5. *SEM micrographs - exogenous inclusion*

3.7. SEM-EDS analysis

EDS analysis reveals that the inclusion is primarily composed of O, Al, Si, and Fe, indicating an oxide-based inclusion, likely aluminosilicate in nature. Such inclusions can act as stress concentrators and contribute to crack initiation at the fracture surface.

Elemental mapping (Figure 7) confirmed that the complex oxide inclusion comprises predominantly of Al, Mg, and Si.

THE ANNALS OF "DUNAREA DE JOS" UNIVERSITY OF GALATI
FASCICLE IX. METALLURGY AND MATERIALS SCIENCE
Nº. 1 - 2026, ISSN 2668-4748; e-ISSN 2668-4756
Article DOI: https://doi.org/10.35219/mms.2026.1.02

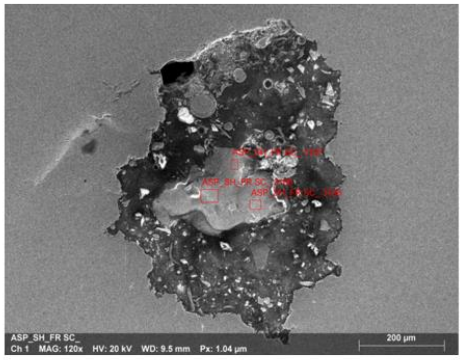

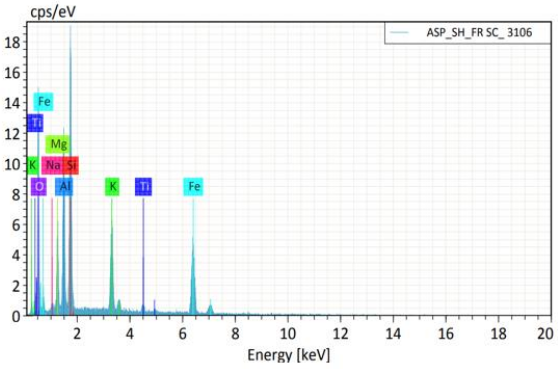

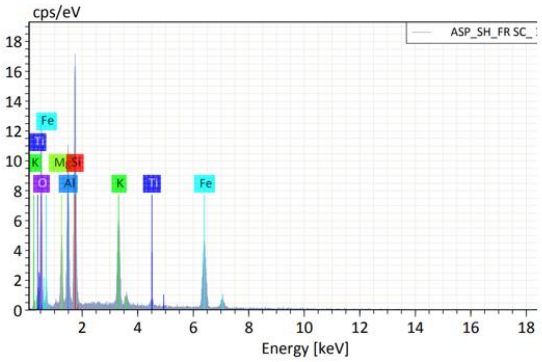

Spectrum	O	Na	Mg	Al	Si	K	Ti	Fe
ASP_SH_FR SC_ 3106	39.91	0.41	5.79	11.22	15.06	7.70	1.01	18.89
ASP_SH_FR SC_ 3107	39.28		4.53	9.93	15.21	8.74	0.91	21.40
ASP_SH_FR SC_ 3108	37.90		5.78	11.88	15.76	8.07	1.12	19.49
Mean	**39.03**	**0.41**	**5.37**	**11.01**	**15.34**	**8.17**	**1.02**	**19.93**
Sigma	**1.03**	**0.00**	**0.73**	**0.99**	**0.37**	**0.53**	**0.11**	**1.31**
SigmaMean	**0.59**	**0.00**	**0.42**	**0.57**	**0.21**	**0.31**	**0.06**	**0.75**

Fig. 6. *EDS spectra*

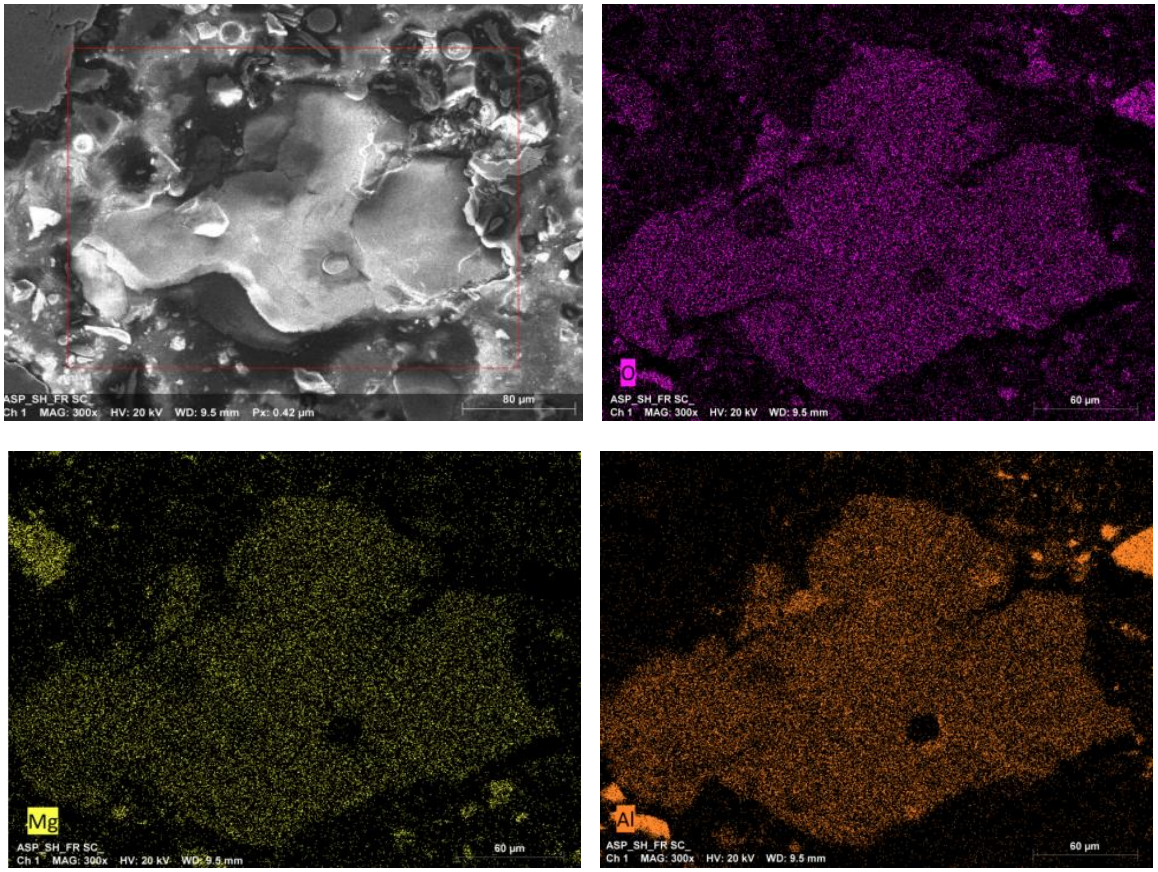

THE ANNALS OF "DUNAREA DE JOS" UNIVERSITY OF GALATI
FASCICLE IX. METALLURGY AND MATERIALS SCIENCE
No. 1 - 2026, ISSN 2668-4748; e-ISSN 2668-4756
Article DOI: https://doi.org/10.35219/mms.2026.1.02

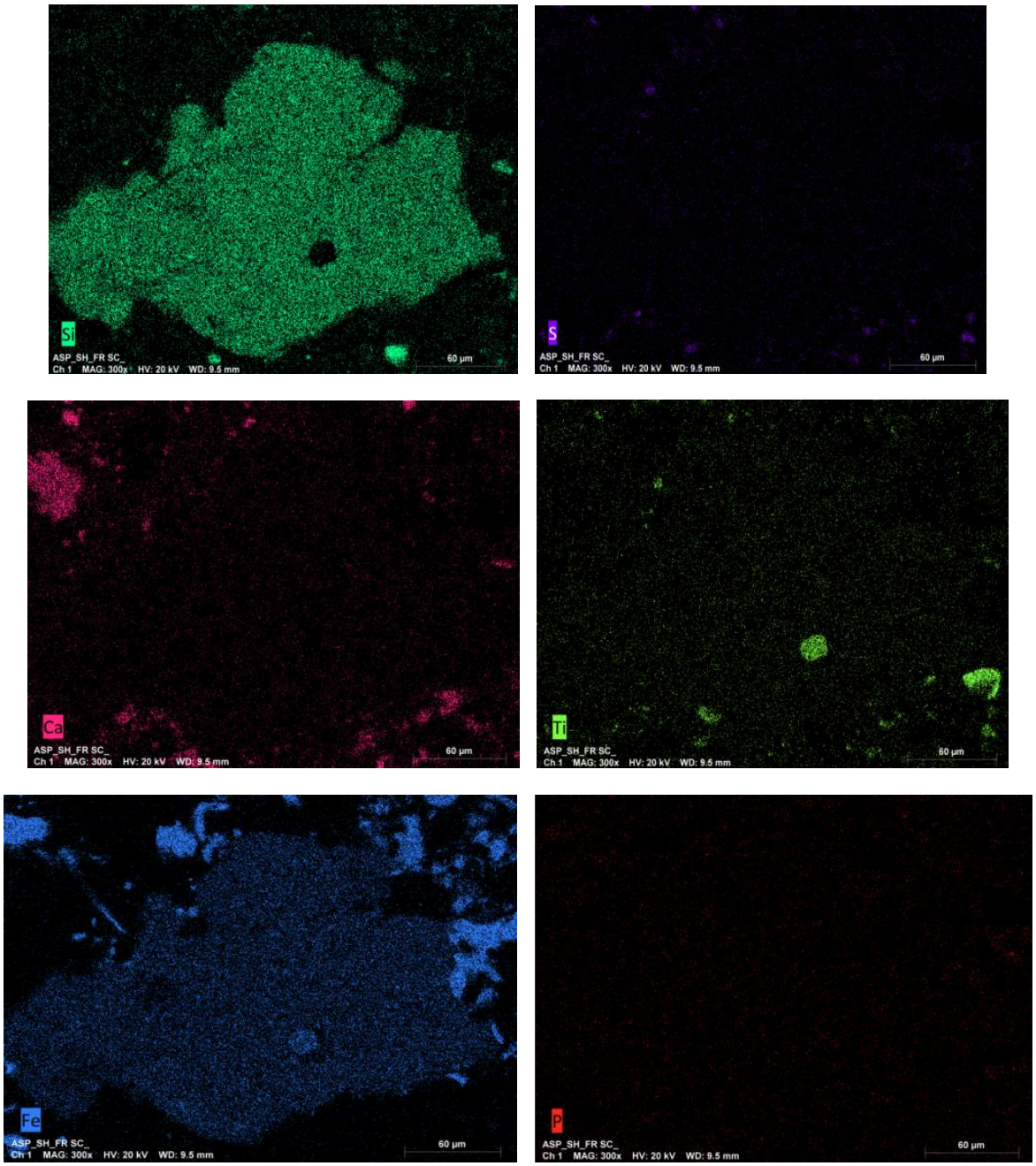

Fig. 7. *Elemental mapping (SEM)*

4. Conclusions

In summary, physical and microscopic examination revealed progressive fatigue features on the fracture surface, including beach marks and ratchet marks. The fracture initiated near the bearing region, and the crack propagated over time under cyclic bending stresses rather than resulting from a sudden overload.

Visual inspection of the housing sleeve showed severe scratches and abrasive wear on the side adjacent to the fractured shaft, confirming significant relative movement due to misalignment of the shaft-bearing assembly. On the opposite side, where no sleeves were installed, remained smooth and free of wear.

Chemical and microstructural analysis showed the shaft material is similar to 42CrMo4 EN10083/3 (2006) steel grade, with the following notable characteristics: a sulphur content of 0.026%, which is on the higher side and prone to harmful inclusions. The lack of calcium addition potentially leaves

inclusions unmodified and elongated, which act as stress concentrators.

SEM-EDS and elemental mapping revealed coarse, complex oxide inclusions (0.72 mm) at the region of initiation.

The defect mechanism and crack progression reveal that misalignment of the shaft-bearing assembly created rotational bending stresses and localized stress concentration zones. Fatigue cracks initiated at stress concentration points under cyclic operational loading were observed. Progressive crack growth is clearly evidenced by beach marks and ratchet marks. Finally, the shaft fracture occurred when the remaining cross-section could no longer sustain the bending loads, with bearing failure occurring subsequently as a secondary event.

Optical microscopy and hardness testing confirmed a homogeneous ferrite–pearlite microstructure, with hardness values consistent with the specified requirements. However, the presence of exogenous complex oxide inclusions and high sulphur levels without calcium treatment indicates a low level of quality focus by the manufacturer, which is concerning for such a critical end-use application.

References

[1]. Hou Nan, *et al.*, *Failure modes, mechanisms and causes of shafts in mechanical equipment*, Engineering Failure Analysis, vol. 136, 106216, 2022.
[2]. Wang M. S., *et al.*, *Failure analysis of screw shaft in screw compressor*, Engineering Failure Analysis, vol. 125, 105424, 2021.
[3]. Shahrivar A., Abdolmaleki A. R., *Failure of a screw compressor shaft*, Engineering Failure Analysis, vol. 13, issue 4, p. 698-704, 2006.
[4]. Florez Jorge Mario Tirado, *et al.*, *Analysis of the failure of an offshore compressor crankshaft*, Case Studies in Engineering Failure Analysis, p. 50-55, 2016.
[5]. Safaat Aat, Noviyanto Alfian, *Failure analysis of rotary screw compressor and its modifications*, International Journal of Innovation in Mechanical Engineering and Advanced Materials, 2021.
[6]. Fioravanti A., *et al.*, *Compressor Station Facility Failure Modes: Causes, Taxonomy and Effects*, Report EUR 30265 EN, by the European Commission Joint Research Centre (JRC), 2020.
[7]. Xu L., *et al.*, *Analysis of the causes of driving gear shaft fractures in gear pumps*, J. Fail. Anal. Prev., 20(1), p. 242-2482020.
[8]. Fuller R.W., *et al.*, *Horstemeyer, Failure analysis of aisi 304 stainless steel shaft*, Eng. Fail. Anal., 15(7), p. 835-846, 2008.
[9]. Callister W. D. Jr., Rethwisch D. G., *Callister's Materials Science and Engineering*, (10th ed.), John Wiley & Sons, 2020.
[10]. Martínez L., *et al.*, *Crack propagation by activated avalanches during creep and fatigue from elastic interface theory*, Physical Review Materials, 9(1), 013401, 2025.
[11]. Singh P., El-Awady J., *Low cycle fatigue behaviour of engineering metallic materials: Review on cyclic deformation micro-mechanism*, Materials Science and Engineering A, 876, 145322, 2024.
[12]. Chen X., *et al.*, *Fatigue life predictor: Predicting fatigue life of metallic materials using LSTM with a contextual attention model*, RSC Advances, 15(3), p. 1234-1247, 2025.
[13]. Rahman M., *et al.*, *Performance of composite metal foams under cyclic loading at elevated temperatures*, Journal of Materials Science, 60(5), p. 2150-2164, 2025.
[14]. Zhao H., *et al.*, *Fatigue crack growth of WC–Co cemented carbides: A comparative study using small indentation flaws and long through-thickness cracks*, International Journal of Fracture, 239(1), p. 1-20, 2024.
[15]. Santos A., *et al.*, *Numerical fatigue crack growth on compact tension specimens under Mode I and mixed-mode (I+II) loading*, Engineering Fracture Mechanics, 290, 110346, 2024.
[16]. Nguyen T., *et al.*, *Elucidating microstructural influences on fatigue behavior for additively manufactured Hastelloy X using a Bayesian-calibrated crystal plasticity model*, Acta Materialia, 266, 118232, 2024.